Stratosphere–troposphere exchange in a changing climate simulated with the general circulation model MAECHAM4

C. Land[1] and J. Feichter

Max-Planck-Institute for Meteorology, Hamburg, Germany

Received 17 May 2002; revised 10 October 2002; accepted 25 November 2002; published 8 March 2003.

[1] Tracer simulations of ^{7}Be and ^{10}Be have been performed with the general circulation model MAECHAM4 for present and future climatic conditions in order to study possible trends of stratosphere–troposphere exchange (STE). These model simulations suggest an intensification of the mean meridional circulation above 100 hPa in a warmer climate. At extratropical tropopause levels, it increases poleward of 60° and between 30°S and the equator. This is attributed to shifts of the transport pattern. Consequently, large-scale STE there increases with time, whereas it decreases between 60°S and 30°S and equatorward of 60°N. STE changes also occur due to changes in eddy activity. Our model results suggest that in a warmer climate cyclonic and blocking-like variability is lower than today poleward of 30°N, and cyclonic activity is stronger at Southern Hemisphere midlatitudes. If the amount of air exchanged per cyclone or cutoff low between stratosphere and troposphere does not change in a warmer climate, our results suggest a decrease of STE poleward of 30°N and an increase at Southern Hemisphere midlatitudes due eddy activity. Extratropical changes in the distributions of ^{7}Be and ^{10}Be are dominated by changes in eddy activity. Due to their short tropospheric lifetime, they are more sensitive to the shorter timescale process. Eddy activity does not play any role in STE in the tropics. Large-scale STE changes there do occur due to changes in the mean meridional circulation. In the troposphere, the zonal mean ^{10}Be/^{7}Be ratio increases in the Southern Hemisphere and decreases in the Northern Hemisphere as a consequence of STE and tropospheric transport changes. Thus, one has to be cautious in using this ratio as an exclusive measure for STE changes because changes in the tropospheric processes can also affect the climatological mean ratio. *INDEX TERMS:* 0305 Atmospheric Composition and Structure: Aerosols and particles (0345, 4801); 1610 Global Change: Atmosphere (0315, 0325); 3319 Meteorology and Atmospheric Dynamics: General circulation; 3362 Meteorology and Atmospheric Dynamics: Stratosphere/troposphere interactions

Citation: Land, C., and J. Feichter, Stratosphere–troposphere exchange in a changing climate simulated with the general circulation model MAECHAM4, *J. Geophys. Res.*, *108*(D12), 8523, doi:10.1029/2002JD002543, 2003.

1. Introduction

[2] Stratosphere–troposphere exchange (STE) is one of the key factors controlling the budgets of ozone, water vapor, and other radiatively active substances in both the troposphere and the stratosphere. It can therefore play a significant role in the radiative forcing of global climate change.

[3] STE occurs on a variety of scales. The large-scale general circulation in the upper troposphere and stratosphere can be described by an organized upwelling from the troposphere to the stratosphere in the tropics [*Plumb*, 1996], isentropic transport to the extratropics in the stratosphere [*Waugh*, 1996], and a downward mass flux from the stratosphere to the troposphere in middle and higher latitudes. This Brewer–Dobson circulation is driven nonlocally by Rossby wave activity in the extratropical middle atmosphere. It acts as a "suction pump," withdrawing air from the tropical troposphere, pushing it poleward and finally downward [*Holton et al.*, 1995]. On the synoptic- and small-scale cutoff lows [*Price and Vaughan*, 1992], tropopause folds, which are associated with cyclogenetic activity [*Van Haver et al.*, 1996], and mixing processes are prominent agents of air mass transfer between stratosphere and troposphere.

[4] In this paper, large-scale STE changes are investigated with the atmosphere general circulation model (GCM) MAECHAM4 by simulating the distributions of the natural radionuclides beryllium-7 (^{7}Be) and beryllium-10 (^{10}Be) for present and future climatic conditions, assuming the Intergovernmental Panel on Climate Change (IPCC) scenario IS92a for changing greenhouse gas (GHG) concentrations. ^{7}Be and ^{10}Be are valuable tracers to evaluate

[1]Now at meteoterra GmbH, Rinteln, Germany.

0148-0227/03/2002JD002543

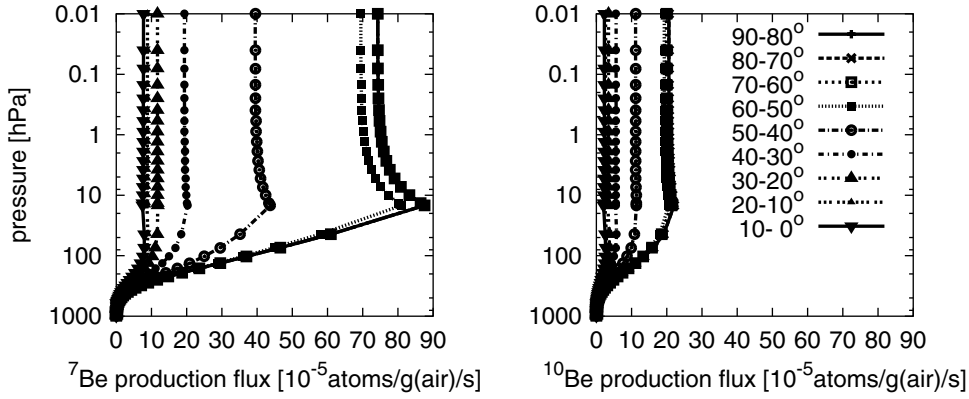

Figure 1. ^{7}Be (left) and ^{10}Be (right) production fluxes for different pressure levels and 10° latitude intervals used in the model simulations. The production fluxes between 60° and 90° plot on top of each other.

the dynamics of two- and three-dimensional regional and global transport models, because they do not interact with radiation, their source sink characteristics are well established, and a relatively large number of observations exist, at least for ^{7}Be. *Rehfeld and Heimann* [1995] simulated the distributions of ^{7}Be, ^{10}Be, ^{222}Rn, and ^{210}Pb to evaluate the dynamics of their ECMWF analysis driven transport model and used the concentration ratio ^{10}Be/^{7}Be as an indicator for STE. They attributed discrepancies between modeled and observed ratios in the Antarctic to deficiencies in the driving wind fields, differences between observed and modeled precipitation, and the scavenging scheme, which was not adequately formulated for this region. Similarly, *Koch and Rind* [1998] calculated the ratio between ^{10}Be and ^{7}Be to investigate STE. In addition, they studied stratospheric transport, focussing on the exchange between the tropics and high latitudes. Their model successfully captured the maximum ^{10}Be/^{7}Be ratio in the lower arctic stratosphere, however, at a lower value. Compared with 1 year of surface observations in the Arctic, stratosphere-to-troposphere transport (STT) in their model seem to be too high and begin too early. They attributed this behavior to excessive springtime leakage into the troposphere.

[5] Large-scale STE changes have already been analyzed by *Butchart and Scaife* [2001] using the Met Office Unified Model and assuming the IPCC scenario IS92a for GHG concentrations. They found an increase of 3% per decade of the mass exchange rate from the tropical troposphere into the stratosphere at 68 hPa.

[6] In the following the setup of our MAECHAM4 model simulations is described first. Then the beryllium distribution of the simulation for present-day is evaluated, followed by an analysis and discussion of STE changes by comparing present and future model climates. Finally, we conclude our results.

2. Model Setup

[7] In this model study, we use the general circulation model MAECHAM4, which is the middle atmosphere version of ECHAM4 [see *Manzini and McFarlane*, 1998, and references therein]. Different to the standard MAECHAM4 model, which applies a semi-Lagrangian transport scheme, we use the advection scheme SPITFIRE [see *Rasch and Lawrence*, 1998]. STE and its changes are studied by simulating the transport of the cosmogenic nuclides ^{7}Be and ^{10}Be for the time slices 2000 and 2100. Sea surface temperatures and the concentration of GHGs (CO_2, CH_4, and N_2O) for the respective years have been taken from a climate response experiment using a coupled atmosphere–ocean general circulation model [*Roeckner et al.*, 1999]. Ozone changes have not been taken into account. The differences between the time slices 2000 and 2100 are exclusively related to different GHG warming.

[8] The production rates of ^{7}Be and ^{10}Be depend on the cosmic ray particle flux. Variations in the geomagnetic field intensity and the solar activity are therefore the dominant causes for time-dependent changes in the production rate. In our simulations we prescribe the ^{7}Be and ^{10}Be production rates according to the studies of *Kollár et al.* [2000] and *Masarik and Beer* [1999], respectively, for long-term mean solar activity, i.e., average solar years, and present geomagnetic field intensity. The production flux depends on the latitude and on the altitude (Figure 1). As the geomagnetic field acts as a shield, the production flux is highest around the magnetic poles and decreases toward lower latitudes. The production rate is zero at the top of the atmosphere. It increases toward the Earth's surface and reaches a maximum above the poles between about 10 and 20 hPa [*Masarik and Beer*, 1999]. As the cosmic ray flux is approximately anticorrelated to the solar activity, the production rate is underestimated (overestimated) in years with weak (strong) solar activity. *Masarik and Beer* [1999] and *Koch et al.* [1996] estimated a range in production estimates due to solar variability of 15–25%. Using these average production rates, the annual global production of ^{7}Be and ^{10}Be for average solar years are 99.47 and 49.19 g/yr, respectively. These values are within the range of production rates given in the literature. *Lal and Peters* [1967] give a global production flux of 151.45 g/yr for ^{7}Be and 120.2 g/yr for ^{10}Be for years with low solar activity. If we add 20% to our production rates to account for low solar activity, the annual global production would be 119.4 and 59.4 g/yr for ^{7}Be and ^{10}Be, respectively. *Masarik and Reedy* [1995] calculated a global ^{7}Be production of 24.12 g/yr and *Oeschger et al.* [1969] determined 37.40 g/yr for ^{10}Be for average solar years.

Table 1. Climatological and Annual Mean Percentage Removal of ^{7}Be by Radiative Decay and Dry and Wet Deposition for 2000 and 2100

^{7}Be	Radiative Decay	Dry Deposition	Wet Deposition
2000	60.7	4.1	35.2
2100	57.5	4.2	38.0

[9] To reduce spin-up times we initialized the concentrations of ^{7}Be and ^{10}Be in the model's stratosphere. For ^{7}Be, secular equilibrium has been assumed. This assumption is justified, because the radioactive half-life of ^{7}Be is relatively short (53 days). The stratospheric concentration of ^{10}Be is mainly determined by transport due to its long half-life of 1.5×10^{6} years. The age distribution as determined with the MAECHAM4 model [*Manzini and Feichter*, 1999] therefore serves as an adequate zonal time pattern to calculate an initial ^{10}Be distribution. We used the same age distribution for all time slices. For ^{7}Be, a spin-up time of 1 year was sufficient to achieve a quasi-steady global burden, for ^{10}Be the spin-up times were 3 years for the time slice 2000 and 5 years for 2100. The last 5 years of each simulation were taken for the analysis.

[10] Very soon after their production, ^{7}Be and ^{10}Be atoms attach to available aerosol particles. Radioactive decay and wet deposition are the most important sinks for ^{7}Be in the atmosphere. Transport into the troposphere and subsequent wet deposition is the main sink for ^{10}Be. A smaller sink results from dry deposition. Wet and dry deposition are parameterized according to the studies of *Feichter et al.* [1991] and *Brost et al.* [1991].

[11] Table 1 displays the climatological and annual mean percentage removal of ^{7}Be by different sinks for 2000 and 2100. For ^{10}Be the percentage removal is 9% and 91% by dry and wet deposition, respectively, in both simulations. For ^{7}Be, an increase in the percentage removal by wet deposition is simulated, which is balanced by a decrease in the percentage removal by radioactive decay.

3. Present-Day Simulation of ^{7}Be and ^{10}Be and Its Evaluation

3.1. Observational Data

[12] Worldwide observations of the ^{7}Be surface concentration have been gathered within the network of the Environmental Measurements Laboratory (EML). They are electronically available via http://www.eml.doe.gov/databases. Five sites, which are able to deliver long data records of at least 20 years, have been selected to evaluate modeled ^{7}Be surface concentrations. Long climatological records of the surface concentration of ^{10}Be are very rare, because its analysis is very expensive. Apart from the ^{10}Be measurements at Zugspitze, Germany, and Jungfraujoch, Switzerland, taken within the STACCATO project, we used ^{10}Be surface concentrations from 1-year measurements at Alert, Canada, by *Dibb et al.* [1994] to evaluate the seasonal cycle of modeled ^{10}Be. For the latter stations, observations of the ^{7}Be surface concentration are also available and the ratio ^{10}Be/^{7}Be can be evaluated as well.

[13] An important sink for ^{7}Be and ^{10}Be is wet deposition. In an evaluation of the modeled surface concentrations of these nuclides, it is useful to investigate observed precipitation fluxes. It has to be kept in mind, however, that it is the precipitation flux along the path to a station that does determine the sink and not necessarily the amount of rainfall at the location of the station. In this study we use the Global Precipitation Climatology Project's (GPCP) Version 2 Combined Precipitation Data Set, which is electronically available from http://www.ncdc.noaa.gov/oa/wmo/wdcamet-ncdc.html/ (see the study of *Huffman* [1997] for a description of the former version of this data set). This data set provides monthly, global $2.5^{\circ} \times 2.5^{\circ}$ gridded fields of two products: the combined satellite-gauge precipitation estimate and the combined satellite-gauge precipitation error estimate. It covers the period January 1979 to the delayed present. The climatological and global mean error amounts 0.9 mm/d. Locally, especially in regions with low amounts of rainfall, the relative error exceeds 80% (not shown). The absolute error may reach 2 mm/d in regions with high amounts of rainfall.

[14] Observational records of ^{7}Be wet deposition fluxes are available in the literature covering mostly short periods of less than 5 years [e.g., *Ishikawa et al.*, 1995; *Koch et al.*, 1996, and references therein; *Papastefanou et al.*, 1995]. Only a few records cover longer periods [e.g., *Igarashi et al.*, 1998] (T. Steinkopff, Deutscher Wetterdienst, Offenbach, Germany, personal communication, 2001). These data have been used to calculate multiyear annual mean values.

3.2. ^{7}Be and ^{10}Be Surface Concentrations

[15] Figure 2 shows the seasonal cycle of climatological ^{7}Be surface concentrations at selected stations. The model is able to capture the seasonality of the ^{7}Be surface concentration at lower latitudes (e.g., at Santiago and Tutuila). At northern polar latitudes, it has difficulties in modeling the high concentrations in winter (e.g., Barrow), which are due to transport from lower latitudes in the so-called Arctic haze period. At the South Pole station, the ^{7}Be surface concentrations are highest in summer and lowest in winter, possibly reflecting the seasonality of subsidence. In the model simulation, the ^{7}Be surface concentration at the South Pole is underestimated by up to 50% in late spring and summer. We did not filter the ^{7}Be observations with respect to the solar influence as was done by *Koch et al.* [1996], because the data records at these stations cover about two solar cycles (22–24 years). At Santiago, the observations cover 28 years from 1970 to 1998. However, climatological mean concentrations are, if at all, only slightly higher than the values in average solar years, because the solar maximum in 1970 was substantially weaker than an average solar maximum.

[16] Figure 3 shows observed and modeled seasonal cycles of the ^{10}Be surface concentration at Alert from 1990/1991 and at the mountain peaks Zugspitze and Jungfraujoch together with the ^{7}Be surface concentration and the ratio ^{10}Be/^{7}Be at the same stations. The ^{10}Be concentrations at Zugspitze and Jungfraujoch are from 2000. ^{7}Be covers the years 1990–1997 at Zugspitze and 1996–2001 at Jungfraujoch. The model is able to simulate the structure of the seasonal cycle of the ^{10}Be surface concentration at Alert. However, maximum concentrations of more than 5.5×10^{4} atoms/m^{3}, which are observed in

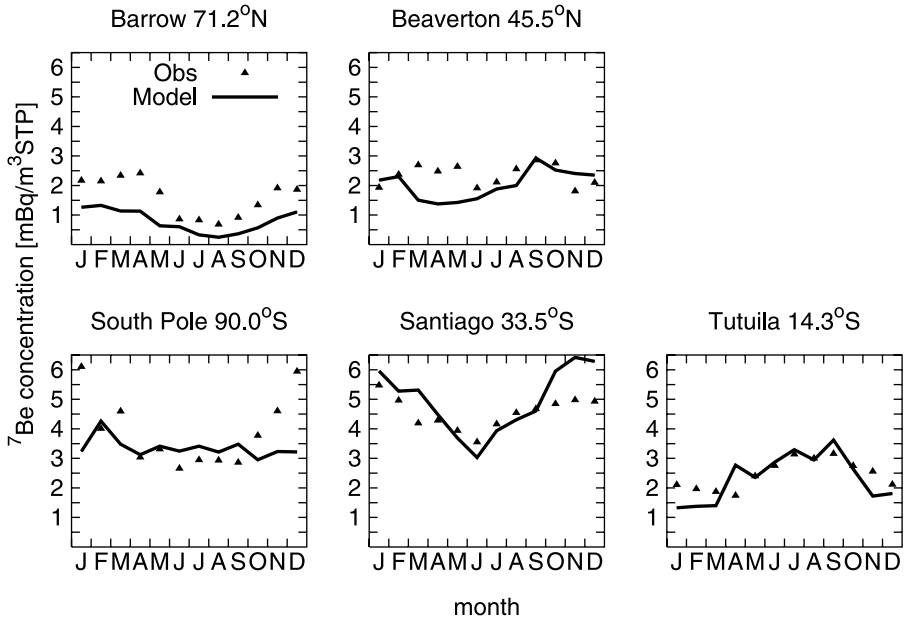

Figure 2. Modeled and observed seasonal cycle of the ^{7}Be surface concentration at selected stations.

northern spring, are not captured by the model simulation. At Zugspitze and Jungfraujoch, modeled ^{10}Be surface concentrations are higher than observed, especially in northern spring and autumn. The modeled ^{7}Be surface concentrations at Alert, Zugspitze, and Jungfraujoch show the same behavior than ^{10}Be surface concentrations, i.e., they deviate from observations in the same seasons, i.e., in northern spring at Alert and additionally in northern autumn at Zugspitze and Jungfraujoch. As a result, the simulated ratio ^{10}Be/^{7}Be is in quite good agreement with observations, because the deviations cancel out. Thus, those processes that mainly determine the climatological mean surface ratio, such as stratospheric transport and STE are captured by the model.

[17] The observations at Alert were taken in a year with maximum solar activity. However, a phase lag of about 4 years between ^{7}Be surface concentrations and the solar flux was calculated by *Koch and Mann* [1996] for Northern Hemisphere stations at the same longitude. Further, at high northern latitudes the observed variability of the ^{7}Be surface concentration is only weakly explained by the solar cycle (about 3% at Alert, Canada). Therefore the observed ^{7}Be surface concentrations at Alert would not be significantly higher than those presented in Figure 3 if they had been adapted to average solar years.

[18] The ^{7}Be surface concentration at Zugspitze and Jungfraujoch cover about half a solar cycle period starting in years

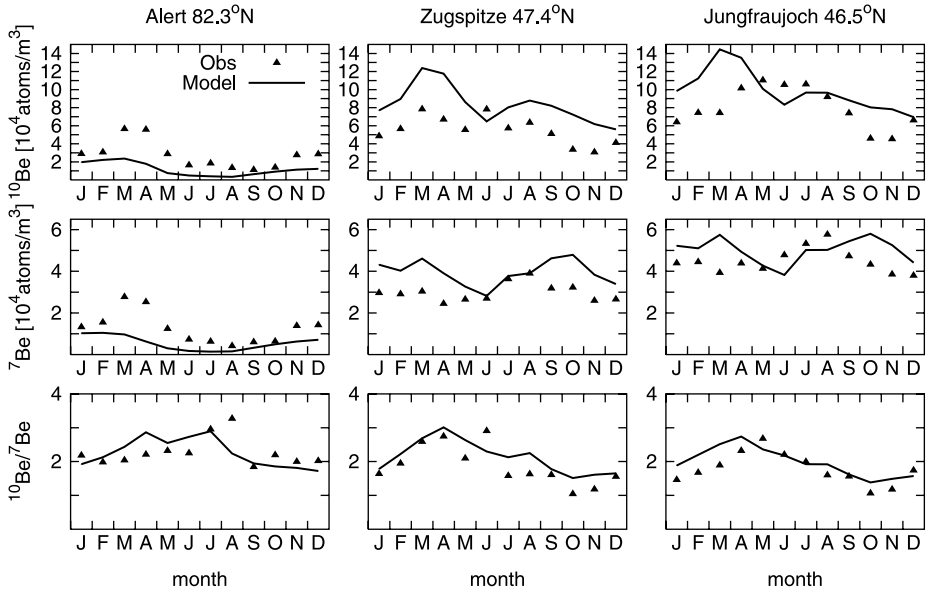

Figure 3. Modeled and observed seasonal cycle of the ^{10}Be surface concentration at Alert, Canada, Zugspitze, Germany, and Jungfraujoch, Switzerland.

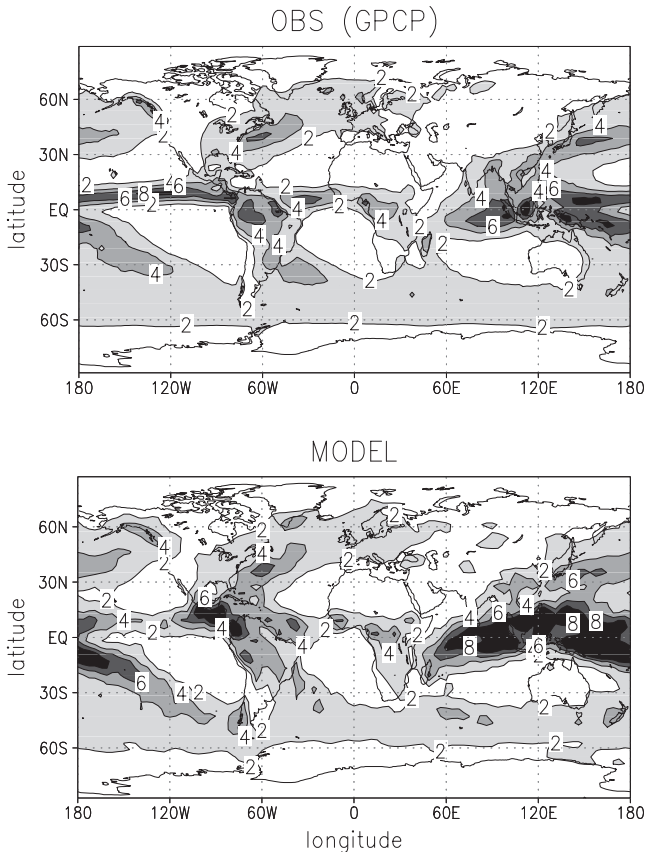

Figure 4. Geographical distribution of observed (top) and modeled (bottom) climatological mean precipitation in mm/d.

with maximum and minimum, respectively, solar activity. Therefore, we do not expect that observation adapted to average solar years would significantly differ from those presented in Figure 3.

[19] As no multiyear observations of ^{10}Be surface concentrations exist, we assume to a first approximation that ^{10}Be surface concentrations are similarly influenced by the solar cycle than ^{7}Be. At Brunswik, Germany, the phase lag between ^{7}Be surface concentrations and the solar flux is about 1 year and the solar cycle explains about 5% of the observed variability of the ^{7}Be surface concentration [*Koch and Mann*, 1996]. Therefore, we would expect slightly higher ^{10}Be surface concentrations at Zugspitze and Jungfraujoch, if they had been adapted to average solar years. As a consequence, the observed ratio ^{10}Be/^{7}Be would be slightly lower.

3.3. Precipitation and Deposition Fluxes

[20] Figure 4 shows modeled and observed climatological and annual mean global distributions of precipitation for present-day.

[21] High amounts of rainfall are observed in the Intertropical Convergence Zone (ITCZ), the South Pacific Convergence Zone (SPCZ), and in the cyclone track regions of the north Pacific and Atlantic (Figure 4, top panel). West of the continents above the cold ocean currents, low rainfall is observed due to subsidence. The geographical distribution of modeled precipitation agrees very well with the observations (Figure 4, bottom). The MAECHAM4 model simulation is able to capture the pattern in precipitation and its magnitude in northern and southern midlatitudes. Differences between observations and model results occur mainly in the ITCZ. Precipitation is stronger than observed in tropical Middle America and along a band extending eastward from Madagascar to the equatorial Pacific. Further, the modeled SPCZ is associated with higher amounts of rainfall than observed. These deviations, however, are mostly within the range of uncertainty of the observations.

[22] Figure 5 shows a scatterplot of observed versus modeled climatological mean ^{7}Be deposition fluxes. At most of the stations, modeled ^{7}Be deposition fluxes agree with the observations within a factor of 2. Only at a few stations in different regions model results and observations differ by more than a factor of 2. However, the range of values is higher in the observations.

4. STE and Climate Change

[23] A large number of simulations with global climate models have been performed to achieve projections of future climate [*Cubasch et al.*, 2001]. There is agreement between these model results that the troposphere warms, the stratosphere cools, and the near surface temperature increases, as a consequence of enhanced GHG concentrations. The simulation results presented in this paper show the same pattern of temperature changes (not shown). The temperature changes are accompanied by changes in the hydrological cycle, namely the globally averaged mean water vapor, evaporation, and precipitation increase. Further, model results suggest that most tropical areas will have increased mean precipitation, most of the subtropical areas will have decreased mean precipitation, and in the high

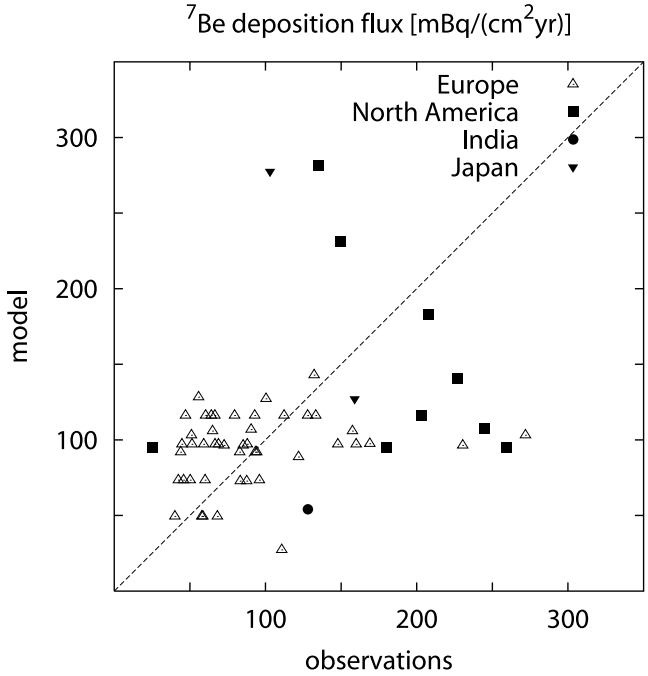

Figure 5. Scatterplot of observed versus modeled climatological mean ^{7}Be deposition flux.

latitudes the mean precipitation will increase. In addition, the intensity of rainfall events will be stronger [*Cubasch et al.*, 2001].

[24] This section discusses changes of those processes that determine changes of ^{7}Be and ^{10}Be surface concentrations and related STE changes. In section 4.1, the mean meridional circulation, which essentially predict the model's meridional transport characteristics, and thus large-scale STE is discussed. Section 4.2 investigates cyclonic and blocking activity at 300 hPa. Sections 4.3 and 4.4 discuss future changes in zonal mean concentration and deposition data of ^{7}Be and ^{10}Be, respectively.

4.1. Transformed Eulerian Mean Meridional Circulation

[25] The residual mean meridional circulation can be regarded as a dynamical tracer to diagnose the model's meridional transport characteristics [*Andrews et al.*, 1987]. The climatological mean residual circulation modeled by MAECHAM4 for a future climate and the relative changes between 2100 and 2000 are shown in Figure 6.

[26] In 2100 tropospheric air enters the stratosphere in the tropics. In the stratosphere it rises further upward and subsequently moves poleward and downward at higher latitudes (Figure 6, top). Above the 100 hPa level northward of 60°S, the modeled climatological mean circulation is significantly stronger in 2100 than in 2000 on both hemispheres (Figure 6, bottom). Thus, the model results suggest an increase of the large-scale transport of ^{7}Be and ^{10}Be northward of 60°S from the stratosphere above 100 hPa into the extratropical atmosphere below 100 hPa with increasing GHG concentrations. At 68 hPa our model simulations predict an increase in mass exchange of 3.2% per decade. These results are in accord with the findings of *Butchart and Scaife* [2001]. For the first half of the 21st century, they predict an increase in mass exchange of 3% per decade at 68 hPa using a global climate model and projected changes in GHG concentrations. Poleward of 60° in the vicinity of the extratropical tropopause (at about 300 hPa) and between 30°S and the equator the residual circulation is higher in 2100 than in 2000. Thus, the large-scale STT shows an increase with time at these latitudes. This increase seems to be related to a horizontal and/or vertical shift in the transport pattern, because the residual circulation stream function decreases at the tropopause equatorward of 60°N and between 60°S and 30°S, and also above this region on the Southern Hemisphere and between about 150 and 250 hPa on the Northern Hemisphere.

4.2. Upper Tropospheric Cyclonic and Blocking-Like Variability

[27] Between 2100 and 2000 the modeled climatological mean meridional temperature gradient on the Northern Hemisphere decreases below 400 hPa and increases in the troposphere above 400 hPa. In the extratropical troposphere, baroclinic eddies develop to reduce meridional temperature gradients. A change in the meridional temperature gradients directly affects baroclinic eddy activity. Further, STE in the extratropics is mainly associated with baroclinic eddies as they are connected with cutoff lows [e.g., *Price and Vaughan*, 1992] and tropopause foldings

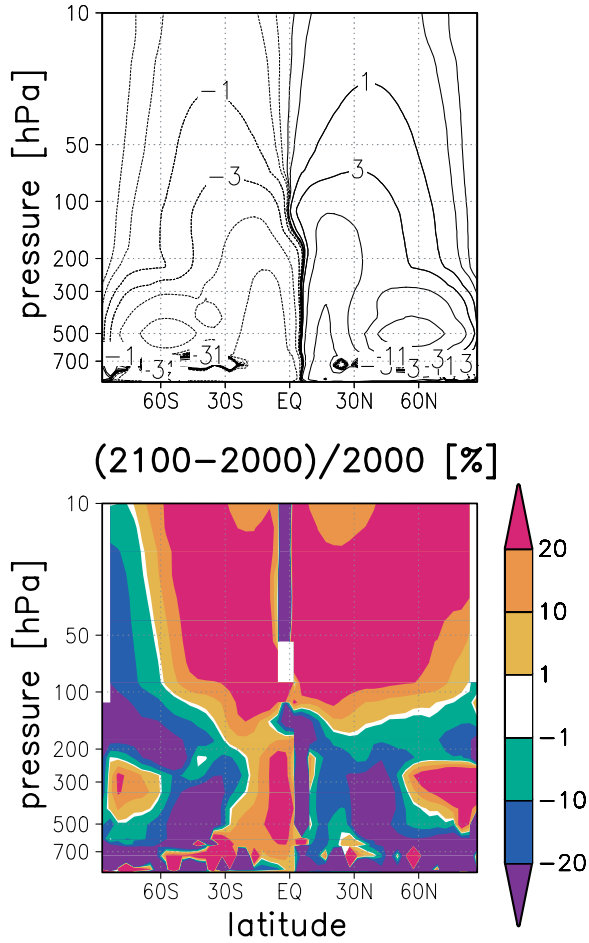

Figure 6. Climatological mean residual circulation stream function in units of 10^{9} kg/s modeled by MAECHAM4 for 2100 (top). Isolines: ±0.1, ±0.3, ±1, ±3, ±10, and ±30. Percentage differences between 2100 and 2000 of the residual mean stream function (bottom).

[e.g., *Van Haver et al.*, 1996]. The standard deviation of daily geopotential height fields from the seasonal mean is most commonly used to represent the strength and spatial structure of cyclonic and blocking-like variability, if the time series are appropriately filtered beforehand. Figure 7 shows the zonal mean of the band-pass (emphasizing timescales between 2.5 and 6 days) and low-pass (emphasizing timescales longer than 10 days) filtered components, respectively, at 300 hPa for northern winter and summer 2000 and the relative difference between 2100 and 2000.

[28] In 2000 cyclones and blocking events occur most frequently poleward of 30° on both winter hemispheres (Figure 7, left). The maximum cyclonic activity occurs at 45°S and at 45°N and 50°N in DJF and JJA, respectively. The strongest blocking-like variability is modeled in JJA at 50°S and 60°N and in DJF at 45°S and 70°N. In 2100 eddy activity on the Northern Hemisphere is weaker than in 2000. Compared to 2000 cyclonic and blocking activity in DJF have significantly decreased by more than 20% at northern polar latitudes in 2100 (Figure 7, right side). In the Southern Hemisphere cyclonic activity in DJF and JJA are about 45% and 20% higher at 60°S and 45°S, respectively

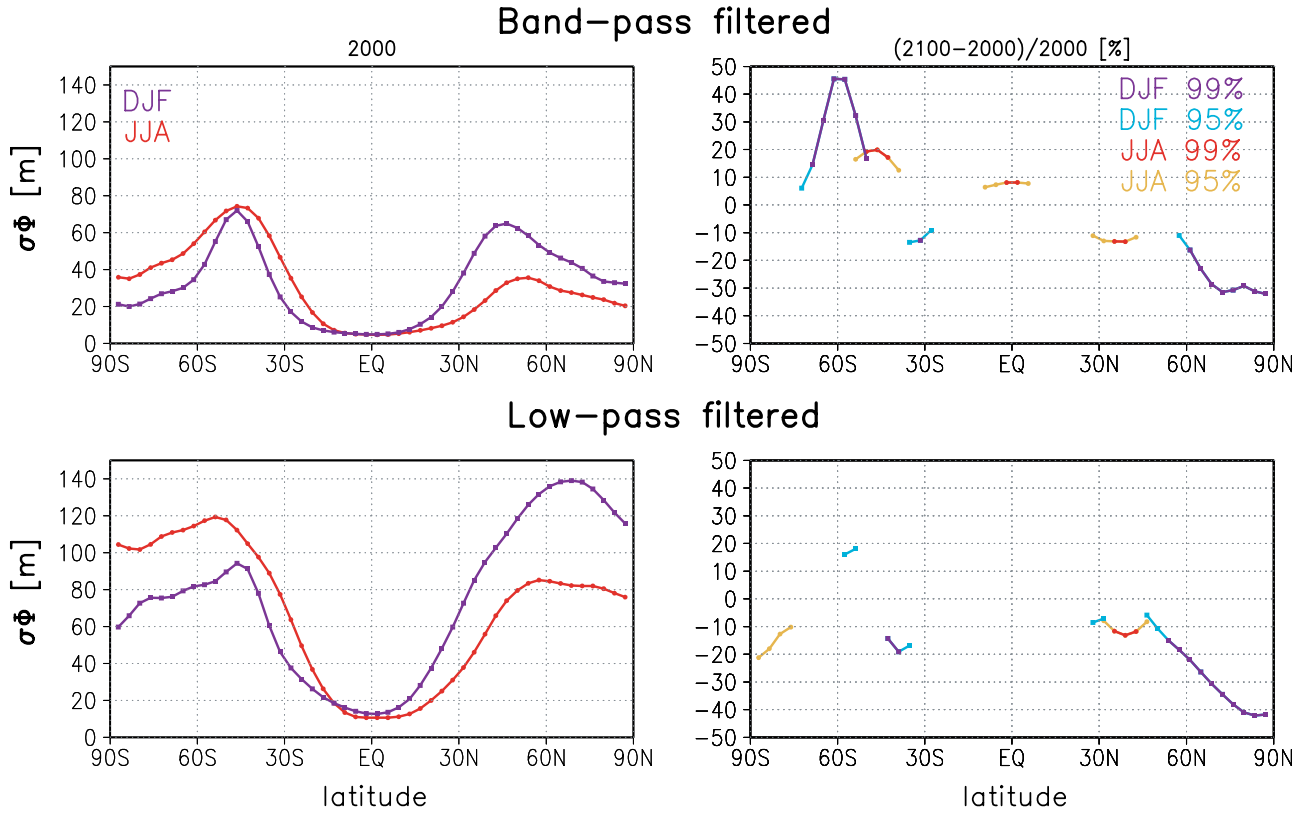

Figure 7. Band-pass and low-pass filtered standard deviation of daily geopotential height fields from the seasonal mean for Northern Hemisphere winter and summer at 300 hPa simulated by MAECHAM4 for 2000 (left) and the relative differences between 2100 and 2000 (right). On the right side, only changes with a significance of at least 95% (Student *t* test) are plotted.

(Figure 7, top right). If we assume that the amount of air exchanged between stratosphere and troposphere per cyclone or cutoff low does not change in the future, our results suggest a decrease of STE poleward of 30°N and an increase at Southern Hemisphere midlatitudes due to eddy activity.

[29] STE changes between 2100 and 2000 occur on the large-scale due to changes in the mean meridional circulation and on the synoptic-scale due to changes in eddy activity. Changes in both processes are responsible for changes in the distributions of ^{7}Be and ^{10}Be. Due to wet deposition the tropospheric lifetime of Be is short compared to its radioactive half-life, namely about 3 weeks. STE changes in the extratropics are therefore dominated by changes in eddy activity, because the timescale associated with it is much shorter than the timescale of the residual circulation. In the tropics, eddy activity does not play any role in STE. Consequently, large-scale STE changes do only occur due to changes in the mean meridional circulation.

4.3. ^{7}Be and ^{10}Be Latitude–Pressure Distributions

[30] Figure 8 shows meridional distributions of the climatological mean concentrations of ^{10}Be and ^{7}Be and the ratio ^{10}Be/^{7}Be for 2000 and the relative differences between 2100 and 2000.

[31] The concentrations of ^{10}Be and ^{7}Be and the ratio are influenced by the residence time in the stratosphere, the STT, and the tropospheric residence time. Due to its shorter radioactive lifetime, the ^{7}Be concentration decreases faster than the ^{10}Be concentration with increasing distance from the source, and thus, the ratio ^{10}Be/^{7}Be increases. Therefore, the stratospheric ratio ^{10}Be/^{7}Be is an indicator for the path-integrated age of an air parcel until it reaches the tropopause. In the troposphere, sources of beryllium are STT and to a minor extent tropospheric production. In the climatological mean, STT of ^{10}Be and ^{7}Be in the model simulation is strongest at about 30° north and south (see Figure 8, top). The tropospheric residence time of Be is short compared to its radioactive lifetime, because wet deposition efficiently removes the aerosols carrying ^{10}Be and ^{7}Be. Therefore, the ^{10}Be and ^{7}Be concentrations and their meridional gradients in the troposphere are low. The ratio ^{10}Be/^{7}Be is high in the stratosphere where the residence time of Be is high and low in the troposphere where the residence time is low. The lowest values of the ratio (<2) occur in the middle tropical troposphere.

[32] Changes in the zonal mean ratio ^{10}Be/^{7}Be between 2100 and 2000 are dominated by changes in the ^{10}Be concentration. Above the 100 hPa level, it decreases by more than 20%. In the troposphere, decreases are simulated poleward of 30°N for ^{10}Be and of 60°N for ^{7}Be and ^{10}Be/^{7}Be. In the Southern Hemisphere troposphere, the ratio ^{10}Be/^{7}Be increases between the equator and 60°S. This is attributable to a stronger increase in the ^{10}Be concentration than in the ^{7}Be concentration.

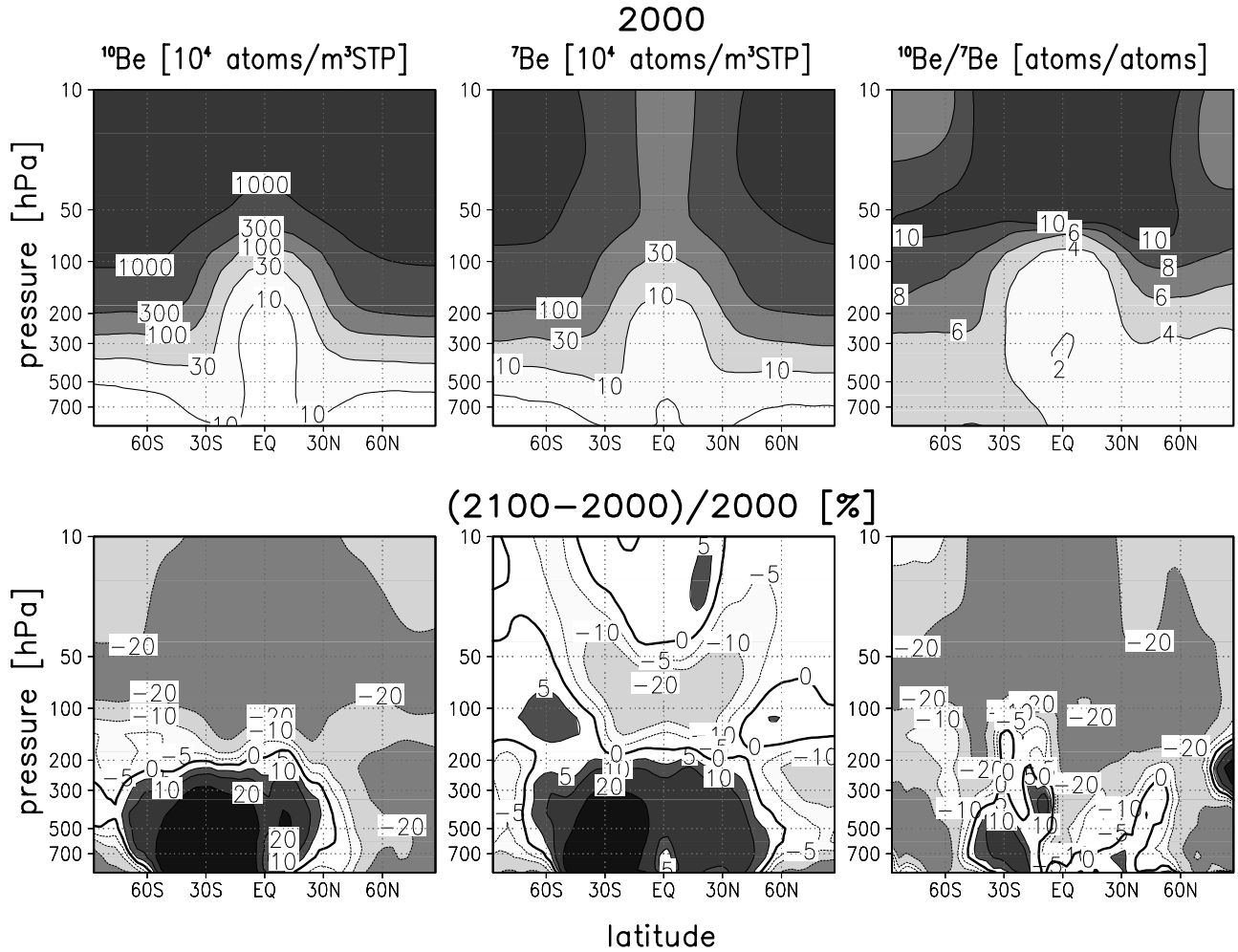

Figure 8. Climatological and zonal mean latitude–pressure distributions of ^{10}Be and ^{7}Be concentration (left and middle, respectively) of the ratio ^{10}Be/^{7}Be (right) modeled by MAECHAM4 for 2000 (top) and the relative differences between 2100 and 2000 (bottom). The zero contour is emphasized.

[33] The concentration changes in the stratosphere can directly be attributed to changes in the mean meridional circulation (see Figure 6). The concentration changes in the troposphere between 2100 and 2000 are dominated by changes in eddy activity. Lower cyclonic and blocking-like variability may have reduced the input of ^{10}Be and ^{7}Be into higher northern tropospheric latitudes. Increased eddy activity on the Southern Hemisphere may have intensified the transport of ^{10}Be and ^{7}Be from the stratosphere into the troposphere. However, in the troposphere not only circulation, but also precipitation changes do occur. The latter are considered in the following subsection together with deposition fluxes of beryllium.

4.4. Zonal Mean Surface Values

[34] In Figure 9, relative changes between 2100 and 2000 of the zonal mean surface concentrations of ^{10}Be and ^{7}Be are depicted together with precipitation and deposition flux variations. The highest relative increase in the surface concentrations of ^{10}Be and ^{7}Be occurs between 30°S and the equator. The ^{10}Be and ^{7}Be surface concentrations are about 30% and 15%, respectively, higher in 2100 than in 2000. The increased surface concentrations are not compensated by reduced sinks. On the contrary, the same latitude region shows increases in ^{10}Be and ^{7}Be deposition fluxes. Therefore, the increased surface concentrations are due to an enhanced supply of beryllium by horizontal and/or vertical transport.

[35] In the Southern Hemisphere between 50°S and the equator precipitation shows only a small increase of 1% between 2100 and 2000. The relative changes in deposition flux of ^{10}Be and ^{7}Be are 1.7% and 3.4%, respectively. Thus, it is likely that the strong relative increase of the surface concentration of ^{10}Be and ^{7}Be between 2100 and 2000 on the Southern Hemisphere can be attributed to increased STT.

[36] In the Northern Hemisphere equatorward of 50°N precipitation decreases (−4%). In this latitude band, ^{10}Be surface concentration and deposition flux changes are lower than 1%, whereas ^{7}Be surface concentration and deposition flux increase by 5% and 2%, respectively. As a consequence, the increase in the ^{7}Be surface concentration is both related to a decrease in precipitation and to increased supply by transport. Poleward of 50°N precipitation increases between 2100 and 2000 by 8%. As the deposition of ^{7}Be and ^{10}Be decreases by −3% and −1%, respectively, this increase in

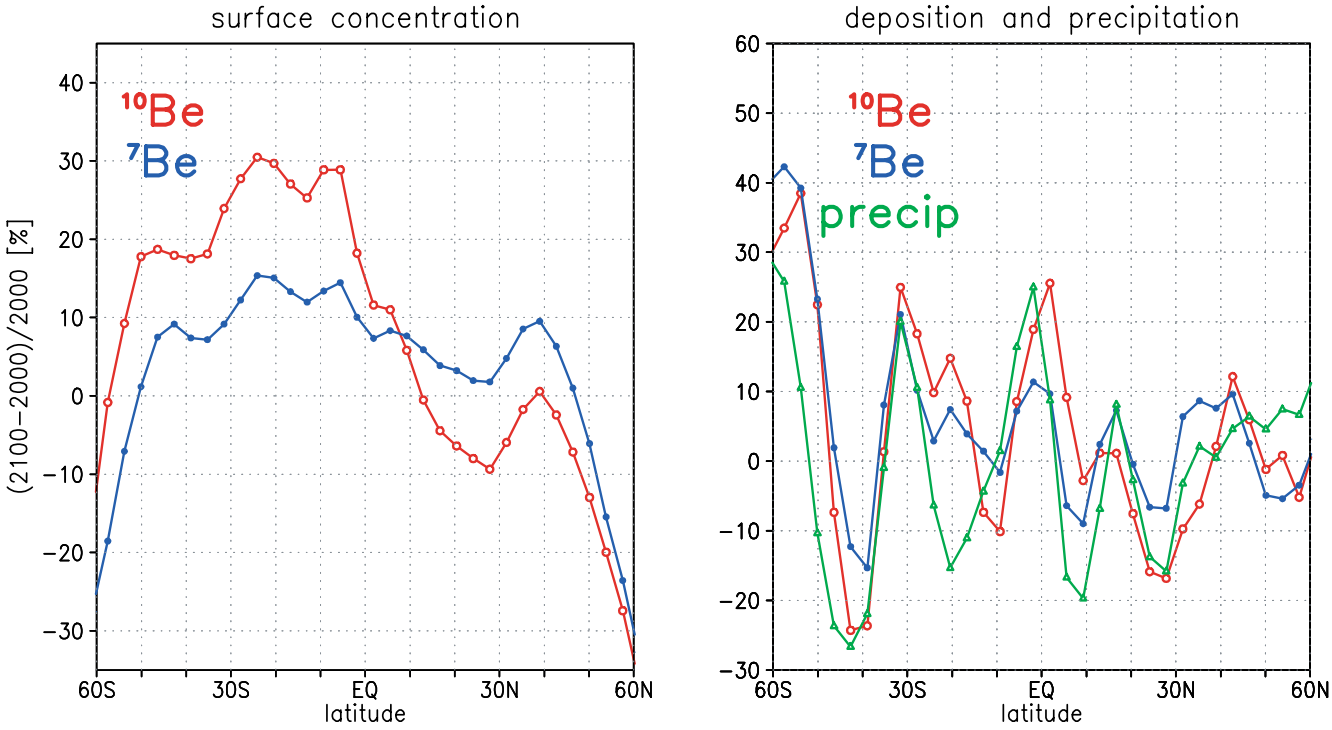

Figure 9. Climatological and zonal mean ^{10}Be and ^{7}Be concentration changes (left) and precipitation and deposition flux changes (right) between 2100 and 2000.

precipitation cannot explain the strong decrease of the ^{7}Be (−18%) and ^{10}Be (−23%) surface concentrations. The decrease in the surface concentrations of ^{7}Be and ^{10}Be has to be attributed to a weakened transport into this area. The decrease in the ratio ^{10}Be/^{7}Be is due to the stronger decrease in ^{10}Be than in ^{7}Be.

5. Conclusions

[37] Tracer simulations of ^{7}Be and ^{10}Be have been performed for present and future climatic conditions with the general circulation model MAECHAM4 to study possible trends of STE. These simulations suggest an intensification of the residual mean meridional circulation above 100 hPa in the future, which is in accord with the results of *Butchart and Scaife* [2001]. At extratropical tropopause level, the residual circulation increases poleward of 60° and between 30°S and the equator, which is attributed to horizontal and/or vertical shifts of the transport pattern. Thus, large-scale STT at these latitudes shows an increase with time, whereas it decreases between 60°S and 30°S and equatorward of 60°N.

[38] STE changes also occur due to changes in eddy activity. Our model results suggest that in the future cyclonic and blocking-like variability will decrease poleward of 30°N and cyclonic activity will increase at Southern Hemisphere midlatitudes. If the amount of air exchanged per cyclone or cutoff low between stratosphere and troposphere does not change in a warmer climate, our results suggest a decrease of STE poleward of 30°N and an increase at Southern Hemisphere midlatitudes due to cyclonic and blocking-like variability. The decrease of upper air cyclonic activity and thus storm track activity in our time slice simulation for 2100 is in contrast to the results obtained by *Ulbrich and Christoph* [1999] from the transient coupled atmosphere–ocean simulation of *Roeckner et al.* [1999]. They found an increasing upper air storm track activity over the east Atlantic and western Europe with rising GHG forcing. However, various investigations using different model data and methods to define the storm track yield remarkably different results [e.g., *Lunkeit et al.*, 1996]. Further, it is still a question of ongoing debate whether low or upper level baroclinicity has a dominating influence on cyclonic activity. Our simulations with MAECHAM4 show a decrease of the meridional temperature gradient and thus baroclinicity below 400 hPa and an increase in the troposphere above 400 hPa on the Northern Hemisphere, leading to a decrease of upper air cyclonic activity in our time slice simulation for 2100.

[39] The tropospheric lifetime of ^{7}Be and ^{10}Be is short compared to their radioactive half-life. STE changes in the extratropics and related changes in the distributions of ^{7}Be and ^{10}Be are therefore dominated by changes in eddy activity, because the timescale associated with it is much shorter than the timescale of the residual circulation. In the tropics, eddy activity does not play any role in STE. Consequently, large-scale STE changes there do only occur due to changes in the mean meridional circulation.

[40] The zonal and climatological mean surface ^{10}Be/^{7}Be ratio increases on the Southern Hemisphere and decreases on the Northern Hemisphere as a consequence of STE changes as well as tropospheric transport changes. Thus, one has to be cautious in using this ratio as an exclusive measure for STE changes, because also changes in the troposphere can affect the climatological mean ratio.

[41] **Acknowledgments.** We thank Michael Ponater from DLR Oberpfaffenhofen, Wessling, for providing the computational package to determine the eddy statistics and Thomas Steinkopff from German Weather Service, Offenbach, for providing ^{7}Be surface activity concentration data and deposition fluxes. The GPCP combined precipitation data were developed and computed by the NASA Goddard Space Flight Center Laboratory for Atmospheres as a contribution to the GEWEX Global Precipitation Climatology project. We are much indebted to Elisa Manzini from Max-Planck-Institute for Meteorology, Hamburg, and two anonymous reviewers for their constructive criticism on the former version of this manuscript. The first author acknowledges funding from EU under grant EVK2-CT-1999-00050.

References

Andrews, D., J. Holton, and C. Leovy (Eds.), *Middle Atmosphere Dynamics*, Academic, San Diego, Calif., 1987.

Brost, R. A., J. Feichter, and M. Heimann, Three-dimensional simulation of ^{7}Be in a global climate model, *J. Geophys. Res.*, *96*, 22,423–22,445, 1991.

Butchart, N., and A. Scaife, Removal of chlorofluorocarbons by increased mass exchange between the stratosphere and troposphere in a changing climate, *Nature*, *410*, 799–802, 2001.

Cubasch, U., G. Meehl, G. Boer, R. Stouffer, M. Dix, A. Noda, C. Senior, S. Raper, and K. Yap, Projections of future climate change, in *Climate Change, 2001: The Scientific Basis, Contribution of Working Group 1 to the Third Assessment Report of the Intergovernmental Panel on Climate Change*, edited by J. Houghton et al., pp. 525–582, Cambridge Univ. Press, New York, 2001.

Dibb, J., L. Meeker, R. Finkel, J. Southon, M. Caffee, and L. Barrie, Estimation of stratospheric input to the arctic troposphere: ^{7}Be and ^{10}Be in aerosols at Alert, Canada, *J. Geophys. Res.*, *99*, 12,855–12,864, 1994.

Feichter, J., R. Brost, and M. Heimann, Three-dimensional modeling of the concentration and deposition of ^{210}Pb, *J. Geophys. Res.*, *96*, 22,447–22,460, 1991.

Holton, J., P. Haynes, M. McIntyre, A. Douglass, R. Rood, and L. Pfister, Stratosphere–troposphere exchange, *Rev. Geophys.*, *33*, 403–439, 1995.

Huffman, G., (Ed.), *The Global Precipitation Climatology Project Monthly Mean Precipitation Data Set*, WMO/TD-808, WMO, Geneva, Switz., 1997.

Ishikawa, Y., H. Murakami, T. Sekine, and K. Yoshihara, Precipitation scavenging studies of radionuclides in air using cosmogenic ^{7}Be, *J. Environ. Radioact.*, *26*, 19–36, 1995.

Koch, D. M., and M. E. Mann, Spatial and temporal variability of ^{7}Be surface concentrations, *Tellus, Ser. B*, *48*, 387–396, 1996.

Koch, D. M., and D. Rind, Beryllium-10/beryllium-7 as a tracer of stratospheric transport, *J. Geophys. Res.*, *103*, 3907–3917, 1998.

Koch, D. M., D. J. Jacob, and W. C. Graustein, Vertical transport of tropospheric aerosols as indicated by ^{7}Be and ^{210}Pb in a chemical tracer model, *J. Geophys. Res.*, *101*, 18,651–18,666, 1996.

Kollár, D., I. Leya, J. Masarik, and R. Michel, Calculation of cosmogenic nuclide production rates in Earth's atmosphere and in terrestrial surface rocks using improved neutron cross sections, *Meteoritics*, *35*, A90–A91, 2000.

Lal, D., and B. Peters, Cosmic ray produced radioactivity on the Earth, in *Handbuch der Physik*, vol. XLVI/2, pp. 551–612, Springer-Verlag, New York, 1967.

Lunkeit, F., M. Ponater, R. Sausen, M. Sogalla, U. Ulbrich, and M. Windelband, Cyclonic activity in a warmer climate, *Contrib. Atmos. Phys.*, *69*, 393–407, 1996.

Manzini, E., and J. Feichter, Simulation of the SF_6 tracer with the middle atmosphere MAECHAM4 model: Aspects of the large-scale transport, *J. Geophys. Res.*, *104*, 31,097–31,108, 1999.

Manzini, E., and N. McFarlane, The effect of varying the source spectrum of a gravity wave parameterization in a middle atmosphere general circulation model, *J. Geophys. Res.*, *103*, 31,523–31,539, 1998.

Masarik, J., and J. Beer, Simulation of particle fluxes and cosmogenic nuclide production in the Earth's atmosphere, *J. Geophys. Res.*, *104*, 12,099–12,111, 1999.

Masarik, J., and R. Reedy, Terrestrial cosmogenic-nuclide production systematic calculated from numerical simulations, *Earth Planet. Sci. Lett.*, *136*, 381–395, 1995.

Oeschger, H., J. Houtermann, H. Loosli, and M. Wahlen, The constancy of cosmic radiation from isotope studies in meteorites and on the Earth, in *Radiocarbon Variations and Absolute Chronology*, edited by I. Olsen, John Wiley, New York, 1969.

Papastefanou, C., A. Ioannidou, S. Stoulos, and M. Manolopoulou, Atmospheric deposition of cosmogenic ^{7}Be and ^{137}Cs from fallout of the Chernobyl accident, *Sci. Total Environ.*, *170*, 151–156, 1995.

Plumb, R., A tropical pipe model of stratospheric transport, *J. Geophys. Res.*, *101*, 3957–3972, 1996.

Price, J., and G. Vaughan, Statistical studies of cut-off low systems, *Ann. Geophys.*, *10*, 96–102, 1992.

Rasch, P., and M. Lawrence, Recent development in transport methods at NCAR, in *MPI Workshop on Conservative Transport Schemes*, edited by B. Machenhauer, Rep. 265, pp. 65–75, Max-Planck-Inst. for Meteorol., Hamburg, Ger., 1998.

Rehfeld, S., and M. Heimann, Three dimensional atmospheric transport simulation of the radioactive tracers ^{210}Pb, ^{7}Be, ^{10}Be, and ^{90}Sr, *J. Geophys. Res.*, *100*, 26,141–26,161, 1995.

Roeckner, E., L. Bengtsson, J. Feichter, J. Lelieveld, and H. Rodhe, Transient climate change simulations with a coupled atmosphere–ocean GCM including the tropospheric sulfur cycle, *J. Clim.*, *12*, 737–754, 1999.

Ulbrich, U., and M. Christoph, A shift of the NAO and increasing storm track activity over Europe due to anthropogenic greenhouse gas forcing, *Clim. Dyn.*, *15*, 551–559, 1999.

Van Haver, P., D. De Muer, M. Beekmann, and C. Mancier, Climatology of tropopause folds at midlatitudes, *Geophys. Res. Lett.*, *23*, 1033–1036, 1996.

Waugh, D., Seasonal variation of isentropic transport out of the tropical stratosphere, *J. Geophys. Res.*, *101*, 4007–4023, 1996.

J. Feichter, Max-Planck-Institute for Meteorology, Bundesstr. 55, D-20146 Hamburg, Germany. (feichter@dkrz.de)

C. Land, meteoterra GmbH, Im Poll 8, D-31737 Rinteln, Germany. (ch.land@meteoterra.de)